Residual γH2AX foci after ex vivo irradiation of patient samples with known tumour-type specific differences in radio-responsiveness

Apostolos Menegakis a,b,⇑, Chiara De Colle d, Ala Yaromina e, Joerg Hennenlotter f, Arnulf Stenzl f, Marcus Scharpf g, Falko Fend g, Susan Noell h, Marcos Tatagiba h, Sara Brucker i, Diethelm Wallwiener i, Simon Boeke a,b, Umberto Ricardi d, Michael Baumann c,j,k,l, Daniel Zips a,b

Department of Radiation Oncology, Medical Faculty and University Hospital, Eberhard Karls University Tübingen; b German Cancer Research Center (DKFZ), Heidelberg and German Consortium for Translational Cancer Research (DKTK) Partner Sites Tübingen; c German Cancer Research Center (DKFZ), Heidelberg and German Consortium for Translational Cancer Research (DKTK) Partner Sites Dresden, Germany; d Department of Oncology, Radiation Oncology, University of Turin, Italy; e Department of Radiation Oncology (Maastro), GROW-School for Oncology and Developmental Biology, Maastricht University Medical Centre, The Netherlands ; f Department of Urology; g Department of Pathology; h Department of Neurosurgery; i Department of and Research Institute for Women's Health, Medical Faculty and University Hospital, Eberhard Karls University Tübingen; j Department of Radiation Oncology, Faculty of Medicine and University Hospital Carl Gustav Carus, Technische Universität; k OncoRay – National Center for Radiation Research in Oncology, Faculty of Medicine and University Hospital Carl Gustav Carus, Technische Universität Dresden; and l Helmholtz-Zentrum Dresden – Rossendorf, Germany

Heterogeneity of tumour radiation response forms the biological basis of personalized radiation oncology. Towards this approach, robust and rapidly available biomarkers informing about the radiobiological characteristics of a given tumour are prerequisite to identify eligible patient subgroups for individualized intervention [1–11]. Among other radiobiological factors, intrinsic radiation sensitivity of tumour cells represents a major component attributing to treatment outcome [3,12–14]. Intrinsic cellular radiation sensitivity correlates with the number of residual unrepaired DNA double strand breaks (DSBs) [15–17]. Therefore, assessment of intrinsic radiation sensitivity through quantification of DNA DSBs has become increasingly utilized in translation cancer research [18–20]. Among other proteins involved in DNA damage response (DDR), the phosphorylated histone variant H2A, i.e. H2AX, has attracted particular attention. Upon irradiation or other exogenous stress, numerous molecules of H2AX are rapidly phosphorylated at the flanking sites of chromatin where DSBs have been induced forming the so-called γH2AX nuclear foci [21–31]. The fact that phosphorylation remains at the sites of DSBs until the end of repair processes before the foci are dephosphorylated [32–36] facilitates the study of foci disappearance along with the quantitative evaluation of residual DSBs [20,21,23,29,37–41]. In several studies both these endpoints have been correlated with cellular radiation sensitivity in vitro and in vivo either in tumour or normal tissue samples [20,21,23,28,29,31,37,39,41,42]. Taking together, the γH2AX assay is simple, sensitive and straightforward method to quantify DSBs in cells and tissues and therefore promising for translation into clinical trials. For clinical application, we have developed and pre-clinically validated a novel method using residual γH2AX foci in ex vivo irradiated tumour specimens [40,43–45]. In the present study we analyse data using the optimizedprotocol in 25 patient-derived surgical specimens (including 7 previously published [45]) covering a spectrum of 10 tumour types with

known differences in radiation response, i.e. radiosensitive types such as seminomas and resistant types as chondrosarcomas. We hypothesized that the number of residual cH2AX foci corresponds to the expected tumour radiation sensitivity. In addition, in order to enhance clinical practicability for future studies the data were used for simulations to test the robustness of the method when omitting dose levels.

Materials and methods

Collection and cultivation of patient-derived tumour specimens

The study has been approved by the Ethics Committee of the Medical Faculty of the University of Tübingen (426/2013BO1). All the patients included in the study were untreated prior to surgical procedure. During collection and cultivation tumour tissues were kept in Dulbecco's MEM culture medium supplemented with 2% HEPES, 1% Na-pyruvate, 1% non-essential amino acids, 1% penicillin streptomycin (all Biochrom AG, Berlin, Germany) and 10% FBS (PAN Biotech GmbH, Aidenbach, Germany). Fresh tumour material was retrieved from surgical specimens and placed in 50 ml Falcon tubes (Becton Dickinson International, Heidelberg, Germany) containing 15 ml culture medium. Tumour specimens were transported to the laboratory and subsequently cut manually with the use of surgical forceps (BD027R, B. BRAUN, Aesculap, Tuttlingen, Germany) and scalpels (FEATHER Safety Razor Co., Ltd., Osaka, Japan Number 23) into approximately 2–3 mm slices before being placed in petri dishes (3.5 cm diameter) coated with a 1.5% agarose layer (A9539, Sigma–Aldrich, Germany) containing 3 ml culture media. During all incubation times the petri-dishes were kept in 95% humidified atmosphere at 37 _C and 5% CO2. For the purpose of the study tumour material from a total of 25 patient tumours with 10 different tumour histologies was collected (Table 1; n = 3 seminomas, n = 1 chondrosarcoma, n = 3 urinary bladder carcinomas (Ca), n = 3 colorectal Ca (2 colon Ca + 1 rectum), n = 3 breast Ca, n = 1 hepatocellular Ca, n = 3 renal cell Ca, n = 3 prostate Ca, n = 4 glioblastoma multiforme (GBM) and n = 2 cervix Ca). In one GBM patient, the specimen was removed from the analysis because in the 0 Gy sample there was no viable tumour part (based on morphological criteria and BrdU positivity) and no estimation of the background foci could be performed. Histology and selection of malignant cells for analysis were confirmed by an experienced pathologist (M.S.).

Experimental design for evaluation of cH2AX foci in ex vivo irradiated patient-derived tumour specimens

The experimental design has been previously described [45]. Briefly, after initial cultivation for 24 h, the tumour specimens were irradiated typically with 0, 2, 4, 6, 8 Gy single doses (200 kV, RS225 research system Gulmay Medical LTD, Surrey, England; 15 mA; 0.5 mm Cu; dose rate _1 Gy/min). In two tumours, additional doses were delivered to the seminoma sample (#1) doses of 3 and 5 Gy and GBM (#1) 10

Gy (both previously published [45]). Prior to irradiation, medium containing 20 lmol pimonidazole (hypoxia marker, Natural Pharmacia International, Belmont, MA, USA) and 10 lmol BrdU (proliferation marker, SERVA electrophoresis, Heidelberg, Germany) was added to the specimens for 4 h (20 h post start of cultivation). Immediately after irradiation, the medium was exchanged. BrdU and pimonidazole were added to visualize the microenvironmental parameters at the time of irradiation, i.e. viability, proliferation and oxygenation. The specimens were further incubated for 24 h before they were fixed in 4% formaldehyde and embedded into paraffin.

Tissue staining, imaging and cH2AX foci analysis

The staining procedure has been previously described [43–45]. In brief, three consecutive 3 lm specimen cross-sections from the paraffin-embedded tumour material were stained for (a) haematoxylin and eosin staining (H&E), (b) BrdU (Clone Bu20a, Dako Deutschland GmbH, Hamburg, Germany) and pimonidazole (Natural Pharmacia International, Belmont, MA, USA; immunohistochemistry, IMH) with ARKTM Kit (animal research kit; Dako Deutschland GmbH, Hamburg, Germany) and (c) 40,6-diamidino- 2-phenylindole (DAPI) and cH2AX at Ser139 (Merck Millipore, Upstate, clone JBW301, Darmstadt, Germany; immunofluorescence IMF) with TSATM Kit (T20912, containing goat anti-mouse IgG and tyramide labelled with Alexa 488, Life Technologies GmbH, Molecular probes, Invitrogen, Darmstadt, Germany). For the evaluation of cH2AX foci a Zeiss Axio Imager Z1 Apotome fluorescence microscope controlled by AxioVision 4.8 software (Carl Zeiss, Jena, Germany) was used as previously described [43–45]. Briefly, complete IMH sections were scanned with a digital colour camera (AxioCamMRc, Rev.3 Fire Wire, Carl Zeiss, Jena, Germany, 100_ (EC Plan Neofluar)) and fields for foci analysis were marked in the scan. In the adjacent IMF section the marked fields were identified and 17 individual images/area were taken every 0.25 lm on the Z-axis (z-stack) using a monochrome digital camera (AxioCamMRm, Carl Zeiss, Jena, Germany; motorized scanning stage, Maerzhaeuser, Wetzlar, Germany, 400_, EC Plan Neofluar). The individual images were fused into a single stack image for foci analysis. For each tumour specimen, five to seven IMF-stacks were taken. Evaluation of cH2AX foci was only performed in intact and viable cell nuclei of well oxygenated tumour cells from the outer rim of the tumour specimen. The pimonidazole border from the IMH scanned section was manually transferred in the corresponding IMF section and 50 cells per dose per patientderived tumour sample from the pimonidazole negative (oxic) specimen area were randomly selected for analysis.

Statistical analysis

The normalized cH2AX foci value was derived as previously reported [45]. In brief, normalization was established to account for aneuploidy, cell cycle effects, partial volume effects and background foci. The normalized foci number (nfoci) per tumour specimen was calculated from,

$$nfoci=(Area_{(m)}/Area_{(i)})*Nfoci_{(i)}-cfoci_{0Gy}$$ nfoci=Area(m)/Area(i)∗Nfoci(i)-cfoci0Gy

where Area(m) is the mean area of all selected nuclei per individual tumour, Area(i) the area of the individual nucleus in which cH2AX foci were evaluated and Nfoci(i) the foci number counted in the corresponding nucleus. For each individual tumour a mean background value of cH2AX cfoci0Gy was determined in sham-irradiated tumour samples. Subsequently the corrected background value of foci was subtracted from the corrected value of each individual cell nucleus counted in the irradiated samples to generate the normalized foci value (nfoci) per nucleus. In case the subtraction was leading to a negative number, the foci value was replaced by zero (0). In order to compare the variability of the residual cH2AX foci numbers across the tumours with different histologies and also within the same tumour histology, an analysis of variance

Table 1.

Characteristics of residual γH2AX nfoci dose response analysis after *ex vivo* irradiation. For each patient-derived specimen, the mean nucleus area included in the calculation of normalized γH2AX foci (nfoci) is depicted. The results of the linear regression analysis of residual γH2AX foci dose response are shown for each individual patient and for each different tumour type. The *p*-value indicates the significance of the linear regression.

Tumour type	**Mean nucleus area (SD) (μm²)**	**Linear regression analysis for each individual tumour**		**Pooled linear regression analysis for each tumour type**	
		Slope (95% C.I.)	***R* squared (r^2)**	**Slope**	***R* squared (r^2)**
Seminoma Classical #1□□	90.1 (23.3)	3.89 (3.55–4.23)	0.56	3.71	0.60
Seminoma Classical #2	94.2 (27.5)	3.69 (3.34–4.03)	0.64		
Seminoma Anaplastic #1□□	94.7 (22.2)	2.64 (2.32–2.96)	0.52	2.64	0.52
Urinary bladder Ca	71.6 (23.0)	1.64 (1.38–	0.39	2.01	0.41

Tumour type	Mean nucleus area (SD) (μm²)	Linear regression analysis for each individual tumour			Pooled linear regression analysis for each tumour type	
		Slope (95% C.I.)		*R* squared (r^2)	Slope	*R* squared (r^2)
#1		1.89)				
Urinary bladder Ca #2	66.9 (18.3)	2.72	(2.46–2.97)	0.64		
Urinary bladder Ca #3	67.3 (18.0)	2.04	(1.75–2.33)	0.44		
Colorectal Ca #1	54.7 (20.9)	2.02	(1.70–2.33)	0.45	1.94	0.40
Colorectal Ca #2	53.4 (20.7)	1.92	(1.45–2.39)	0.29		
Colorectal Ca #3	60.1 (24.7)	1.92	(1.71–2.13)	0.40		
Breast Ca #1	54.7 (20.6)	1.61	(1.41–1.79)	0.53	1.68	0.45
Breast Ca #2	56.1 (13.4)	1.45	(1.24–1.66)	0.43		
Breast Ca #3	62.0 (26.5)	1.99	(1.70–2.24)	0.45		
Hepatocellular Ca #1	64.8 (18.6)	1.86	(1.61–2.11)	0.48	1.56	0.26
Renal cell carcinoma #1	49.3 (10.1)	1.48	(1.27–1.69)	0.44	1.54	0.41
Renal cell carcinoma #2	50.9 (11.8)	1.80	(1.56–2.03)	0.47		
Renal cell carcinoma #3	39.3 (7.1)	1.38	(1.19–1.55)	0.48		
Prostate Ca #1	50.0 (11.0)	0.83	(0.72–	0.51	1.41	0.61

Tumour type	Mean nucleus area (SD) (μm²)	Linear regression analysis for each individual tumour		Pooled linear regression analysis for each tumour type	
		Slope (95% C.I.)	*R* squared (r^2)	Slope	*R* squared (r^2)
		0.93)			
Prostate Ca #2	51.6 (11.0)	2.18 (1.88–2.47)	0.46		
Prostate Ca #3	53.8 (12.6)	1.19 (1.04–1.32)	0.53		
GBM #1	54.2 (12.1)	1.24 (0.97–1.51)	0.20	1.07	0.21
GBM #2	57.5 (12.0)	0.62 (0.44–0.80)	0.16		
GBM #3	67.2 (21.9)	1.18 (1.00–1.37)	0.38		
Cervix Ca #1	57.4 (15.5)	0.58 (0.42–0.74)	0.21	0.99	0.23
Cervix Ca #2	58.0 (18.5)	1.18 (0.93–1.44)	0.25		
Chondrosarcoma #1	47.5 (15.9)	0.74 (0.57–0.92)	0.22	0.69	0.17

p-Value < 0.0001.

Previously published.

(ANOVA) test was performed (Sheffe test for multiple comparisons). For the simulation analysis slopes for individual tumours were calculated omitting various dose levels and the ranking of radiation sensitivity was then compared to the ranking based on the slope estimated from the full dose response. Statistical analysis was performed with STATA 11.0 (STATA Corporation, CollegeStation, TX, USA) and graphs were plotted with GraphPad Prism 6 (GraphPad Software, Inc. San Diego, CA, USA). Fit comparison was done with likelihood-ratio tests and p-values <0.05

were considered statistically significant. Fit comparisons were performed using raw data and mean values along with error bars are reported for visualization purpose.

Results

Characteristics of the patient-derived tumour specimens

All the tumour samples expressed a typical staining pattern for BrdU and pimonidazole, i.e. with the outer rim of the specimen being predominantly pimonidazole-negative and BrdU-positive (data not shown). In total, tumour samples from 25 patients with 10 different tumour types were retrieved and 125 tumour biopsy-specimens were analysed for residual cH2AX foci (Table 1). This includes data from 7 previously published samples [45]. In all the tumours a normal (Gaussian) frequency distribution of the nucleus area per each tumour was observed (data not shown). There was no systematic difference of the nucleus area across the different doses within each individual tumour (data not shown). Therefore a mean value of nucleus area over all doses for each individual tumour was used. The values of nuclear area ranged from 39.3 lm2 (SD: 7.1) for renal cell Ca to 94.2 lm2 (SD: 22.2) for anaplastic seminoma (Table 1). For the calculation of the normalized residual cH2AX foci value a mean ‘‘background” foci value was used from each tumour calculated from the cH2AX foci in the sham-irradiated controls. The background cH2AX foci values ranged from zero for urinary bladder cancer (#3) and colorectal cancer (#1) to 2.58 (SD: 2.69) for GBM (#3)(data not shown).

Dose–response of residual cH2AX foci in ex vivo irradiated patientderived tumour samples

Fig. 1 depicts a representative staining pattern of residual cH2AX foci 24 h post 4 Gy irradiation for each tumour type. In all tumour samples a significant linear increase of residual cH2AX foci with increasing radiation dose was observed and the slope of the dose–response as parameter of intrinsic radiation sensitivity was derived (Fig. 2). In Fig. 3 the tumour types are ranked according to their slope values with at one end of the spectrum the sensitive types such as seminomas with large slope values indicating high number of residual foci and on the other hand resistant tumour types such as sarcoma and GBM with small slope values. ANOVA with Sheffe correction of the pooled slope data per tumour type (Table 1) revealed that the variance within a given tumour type is less pronounced than across different types (Sum of Squares (SS) between groups: 19.8, SS within groups: 2.4; $p < 0.0001$). Simulation analysis of slope estimation and number of dose levels To explore whether the labour-intense manual microscopy visualization and quantification of cH2AX foci with five different dose levels can be simplified without compromising robustness, we used the datasets to perform simulations where dose levels were systematically excluded and the slopes were compared to the slopes estimated from full dose–response relationship considered as reference. Five different scenarios with one to three dose levels were analysed. Based on the slope of full dose response patients were stratified

into sensitive (>75% percentile), moderate (25–75% percentile) or resistant (<25% percentile; Supplementary Fig. 1). The ranking method is arbitrary and was established empirically due to a lack of standardization. This stratification was used for comparison with the other scenarios (0–4–8 Gy, 0–2–4 Gy, 0–2–6 Gy, 0–6 Gy, 0–8 Gy). The results are summarized in
Supplementary Tables 2–6 and Figs. 2–6 and suggest that dose levels might be omitted without major changes in the stratification as long as high doses such as 6 or 8 Gy are included.

Discussion

In the present study we applied our optimized protocol of the cH2AX ex vivo assay to determine intrinsic radiation sensitivity in 25 samples from 10 different tumour types with known differences in tumour radiation sensitivity. The analysis includes previously published data from 7 samples [45]. The slopes of the residual cH2AX foci dose–response curves were different by a factor of more than five across the tumour types (Fig. 3). Importantly, the ranking of the slopes was found to be consistent with the expected radio-responsiveness, i.e. high values in sensitive tumour types such as seminomas and low values in resistant tumour types such as chondrosarcomas and GBM [46–48]. This finding supports the initial hypothesis that the cH2AX ex vivo data correlate with expected radio-responsiveness in a panel of sensitive, moderate and resistant tumours types. The data also support the concept that intrinsic radiation sensitivity of tumour cells contribute to tumour radiation response while there is large overlap between different tumour types. It is important to note that also other radiobiological factors such as tumour hypoxia contribute to tumour radiation response and need to be assessed in order to precisely
predict outcome. Our assay is specifically optimized to assess intrinsic radiation sensitivity without being affected by alterations of the microenvironment ex vivo during sampling and cultivation. In the present study, no attempts were made to assess the extentof tumour hypoxia in situ. Conceptually, intrinsic radiation sensitivity is assessed under oxygenated conditions in the outer rim of
the ex vivo reoxygenated specimen [45]. Pimonidazole and BrdU were only added to assure that foci are counted solely in viable, proliferating and well oxygenated tumour areas. For future studies it will become important to combine tests of intrinsic radiation sensitivity with hypoxia assessment [49] and gene signatures [50], e.g. by functional imaging or gene expression profiles, and other biomarkers. We have recently started a prospective trial to develop a decision-support-model in head and neck cancer patients including cH2AX ex vivo foci assay, functional imaging,
radiomics, genomics and clinico-pathological factors. In the first step, we prospectively collect data for creating predictive models using systems biology approaches and advanced data science. In a second step, we will independently validate the model using biopsies and surgical specimens for future interventional studies, i.e. assigning individual radiation dose with or without prior surgery. To our knowledge we present here first dataset on a panel of tumour types using the cH2AX

ex vivo foci assay to determine radiation sensitivity. Similarly, freshly excised tumour material for functional tests have been used by others. Tumour samples from breast cancer patients were ex vivo irradiated and the subsequentformation of RAD51 foci was used to detect defects in homologous recombination repair (HRR) of DSBs to identify patients for PARP inhibition [51]. Importantly, in contrast to our method the Rad51 assay is specific for HRR and was not aimed to determine radiation sensitivity across different tumour types. Similar experiments have been performed in patient-derived ovarian cancer xenografts [52]. Differences in intrinsic radiation sensitivity across and among different tumour types have been shown before with the SF2 assay, i.e. the surviving fraction after 2 Gy [12–14]. Overall, it appears that our first data in 10 different tumour types are in line with the SF2 experience. Despite the promising results and the potential for patient stratification [53,54] the SF2 assay was not further developed to be integrated in clinical trials testing individualized radiation oncology. This was among other reasons due to technical and methodological issues resulting in a limited success rate and a long duration of the assay. We believe that the proposed ex vivo γH2AX assay presented here can overcome these limitations by providing rapid results (within few days) at a very high success rate. In addition, the ex vivo γH2AX assay can further be optimized towards higher clinical practicability such as the use of automated microscope counting software [55,56] and the omission of dose levels without compromising robustness (Suppl. Figs. 1–6). The latter analysis is limited by the fact that the ranking system used was arbitrarily and empirically defined as no standardized reference system exists. Further limitations of the present studies include sampling error, sample size and lack of external validation, potential effects of the ex vivo manipulation of the tissues. While the present study demonstrates large differences in intrinsic radiation sensitivity across different tumour types, the next step towards utilizing the assay for personalized radiation oncology would be to apply it in a sufficiently large number of tumours of the same type and correlate the data with established clinic-pathological parameters and patient outcome. Furthermore, the accuracy of the assay will critically depend on the variability of intrinsic radiation sensitivity across an individual tumour, i.e. on the sampling error. Both issues are addressed in an ongoing study in a cohort of prostate cancer patients. In conclusion, we confirm the clinical feasibility of the γH2AX ex vivo assay. The slopes of the residual foci number per dose unit are well in line with the expected differences in radioresponsiveness of different tumour types implying that intrinsic radiation sensitivity contributes to tumour radiation response. Thus, this assay has a promising potential for individualized radiation oncology and prospective validation is warranted.

Financial support

This study was supported by the Applied Clinical Research (AKF-Angewandte Klinische Forschung) program (Medical Faculty Tuebingen, project number E.03.35204.2) and by the German Consortium for Translational Cancer Research (DKTK) partner site Tübingen.

Conflict of interest

The authors have no conflict of interest to declare.

Acknowledgments

The authors wish to thank Dennis Thiele for excellent technical assistance, and Dr. Pericles Kosmidis for retrieving the pathology reports of the patients and thus assisting in verifying the histology of each individual tumour.

References

[1] Bibault JE, Fumagalli I, Ferte C, Chargari C, Soria JC, Deutsch E. Personalized radiation therapy and biomarker-driven treatment strategies: a systematicreview. Cancer Metastasis Rev 2013;32:479–92.
[2] Ree AH, Redalen KR. Personalized radiotherapy: concepts, biomarkers and trial design. Br J Radiol 2015;88:20150009.
[3] Yaromina A, Krause M, Baumann M. Individualization of cancer treatment from radiotherapy perspective. Mol Oncol 2012;6:211–21.
[4] Bentzen SM, Gregoire V. Molecular imaging-based dose painting: a novel paradigm for radiation therapy prescription. Semin Radiat Oncol 2011;21:101–10.
[5] Butof R, Dubrovska A, Baumann M. Clinical perspectives of cancer stem cell research in radiation oncology. Radiother Oncol 2013;108:388–96.
[6] Lohaus F, Linge A, Tinhofer I, Budach V, Gkika E, Stuschke M. HPV16 DNA status is a strong prognosticator of loco-regional control after postoperative radiochemotherapy of locally advanced oropharyngeal carcinoma: results from a multicentre explorative study of the German Cancer Consortium Radiation Oncology Group (DKTK-ROG). Radiother Oncol 2014.
[7] Martens MH, Subhani S, Heijnen LA, Lambregts DM, Buijsen J, Maas M, et al. Can perfusion MRI predict response to preoperative treatment in rectal cancer? Radiother Oncol 2015;114:218–23.
[8] Nijkamp MM, Span PN, Terhaard CH, Doornaert PA, Langendijk JA, van den Ende PL, et al. Epidermal growth factor receptor expression in laryngeal cancer predicts the effect of hypoxia modification as an additive to accelerated radiotherapy in a randomised controlled trial. Eur J Cancer 2013;49:3202–9.
[9] Valentini V, van Stiphout RG, Lammering G, Gambacorta MA, Barba MC, Bebenek M, et al. Selection of appropriate end-points (pCR vs 2yDFS) for tailoring treatments with prediction models in locally advanced rectal cancer. Radiother Oncol 2015;114:302–9.
[10] Someya M, Yamamoto H, Nojima M, Hori M, Tateoka K, Nakata K, et al. Relation between Ku80 and microRNA-99a expression and late rectal bleeding

after radiotherapy for prostate cancer. Radiother Oncol 2015;115:235–9.
[11] Coroller TP, Grossmann P, Hou Y, Rios Velazquez E, Leijenaar RT, Hermann G, et al. CT-based radiomic signature predicts distant metastasis in lung adenocarcinoma. Radiother Oncol 2015;114:345–50.
[12] Deacon J, Peckham MJ, Steel GG. The radioresponsiveness of human tumours and the initial slope of the cell survival curve. Radiother Oncol 1984;2:317–23.
[13] Fertil B, Malaise EP. Inherent cellular radiosensitivity as a basic concept for human tumor radiotherapy. Int J Radiat Oncol Biol Phys 1981;7:621–9.
[14] Malaise EP, Fertil B, Chavaudra N, Guichard M. Distribution of radiation sensitivities for human tumor cells of specific histological types: comparison of in vitro to in vivo data. Int J Radiat Oncol Biol Phys 1986;12:617–24.
[15] Dikomey E, Brammer I. Relationship between cellular radiosensitivity and non-repaired double-strand breaks studied for different growth states, dose rates and plating conditions in a normal human fibroblast line. Int J Radiat Biol 2000;76:773–81.
[16] Wada S, Van Khoa T, Kobayashi Y, Funayama T, Ogihara K, Ueno S, et al. Prediction of cellular radiosensitivity from DNA damage induced by gammarays and carbon ion irradiation in canine tumor cells. J Vet Med Sci 2005;67:1089–95.
[17] Jackson SP. Sensing and repairing DNA double-strand breaks. Carcinogenesis 2002;23:687–96.
[18] Ivashkevich A, Redon CE, Nakamura AJ, Martin RF, Martin OA. Use of the gamma-H2AX assay to monitor DNA damage and repair in translational cancer research. Cancer Lett 2012;327:123–33.
[19] Redon CE, Weyemi U, Parekh PR, Huang D, Burrell AS, Bonner WM. Gamma-H2AX and other histone post-translational modifications in the clinic. Biochim Biophys Acta 2012;1819:743–56.
[20] Sak A, Stuschke M. Use of gammaH2AX and other biomarkers of double-strand breaks during radiotherapy. Semin Radiat Oncol 2010;20:223–31.
[21] Olive PL, Banath JP. Phosphorylation of histone H2AX as a measure of radiosensitivity. Int J Radiat Oncol Biol Phys 2004;58:331–5.
[22] Rogakou EP, Pilch DR, Orr AH, Ivanova VS, Bonner WM. DNA double-stranded breaks induce histone H2AX phosphorylation on serine 139. J Biol Chem 1998;273:5858–68.
[23] Bonner WM, Redon CE, Dickey JS, Nakamura AJ, Sedelnikova OA, Solier S, et al. GammaH2AX and cancer. Nat Rev Cancer 2008;8:957–67.
[24] Downs JA. Chromatin structure and DNA double-strand break responses in cancer progression and therapy. Oncogene 2007;26:7765–72.
[25] Downs JA, Cote J. Dynamics of chromatin during the repair of DNA doublestrand breaks. Cell Cycle 2005;4:1373–6.
[26] Downs JA, Nussenzweig MC, Nussenzweig A. Chromatin dynamics and the preservation of genetic information. Nature 2007;447:951–8.
[27] Fillingham J, Keogh MC, Krogan NJ. GammaH2AX and its role in DNA doublestrand break repair. Biochem Cell Biol 2006;84:568–77.
[28] Hunt CR, Ramnarain D, Horikoshi N, Iyengar P, Pandita RK, Shay JW, et al.

Histone modifications and DNA double-strand break repair after exposure to ionizing radiations. Radiat Res 2013;179:383–92.
[29] Kinner A, Wu W, Staudt C, Iliakis G. Gamma-H2AX in recognition and signaling of DNA double-strand breaks in the context of chromatin. Nucleic Acids Res 2008;36:5678–94.
[30] Scully R, Xie A. Double strand break repair functions of histone H2AX. Mutat Res 2013;750:5–14.
[31] Turinetto V, Giachino C. Multiple facets of histone variant H2AX: a DNA double-strand-break marker with several biological functions. Nucleic Acids Res 2015;43:2489–98.
[32] Chowdhury D, Keogh MC, Ishii H, Peterson CL, Buratowski S, Lieberman J. Gamma-H2AX dephosphorylation by protein phosphatase 2A facilitates DNA double-strand break repair. Mol Cell 2005;20:801–9.
[33] Downey M, Durocher D. GammaH2AX as a checkpoint maintenance signal. Cell Cycle 2006;5:1376–81.
[34] Keogh MC, Kim JA, Downey M, Fillingham J, Chowdhury D, Harrison JC, et al. A phosphatase complex that dephosphorylates gammaH2AX regulates DNA damage checkpoint recovery. Nature 2006;439:497–501.
[35] Nakada S, Chen GI, Gingras AC, Durocher D. PP4 is a gamma H2AX phosphatase required for recovery from the DNA damage checkpoint. EMBO Rep 2008;9:1019–26.
[36] Moon SH, Nguyen TA, Darlington Y, Lu X, Donehower LA. Dephosphorylation of gamma-H2AX by WIP1: an important homeostatic regulatory event in DNA repair and cell cycle control. Cell Cycle 2010;9:2092–6.
[37] Banath JP, Klokov D, MacPhail SH, Banuelos CA, Olive PL. Residual gammaH2AX foci as an indication of lethal DNA lesions. BMC Cancer 2010;10:4.
[38] Banath JP, Macphail SH, Olive PL. Radiation sensitivity, H2AX phosphorylation, and kinetics of repair of DNA strand breaks in irradiated cervical cancer cell lines. Cancer Res 2004;64:7144–9.
[39] Klokov D, MacPhail SM, Banath JP, Byrne JP, Olive PL. Phosphorylated histone H2AX in relation to cell survival in tumor cells and xenografts exposed to single and fractionated doses of X-rays. Radiother Oncol 2006;80:223–9.
[40] Menegakis A, Yaromina A, Eicheler W, Dorfler A, Beuthien-Baumann B, Thames HD, et al. Prediction of clonogenic cell survival curves based on the number of residual DNA double strand breaks measured by gammaH2AX staining. Int J Radiat Biol 2009;85:1032–41.
[41] Olive PL. Retention of gammaH2AX foci as an indication of lethal DNA damage. Radiother Oncol 2011;101:18–23.
[42] Banuelos CA, Banath JP, Kim JY, Aquino-Parsons C, Olive PL. GammaH2AX expression in tumors exposed to cisplatin and fractionated irradiation. Clin Cancer Res 2009;15:3344–53.
[43] Koch U, Hohne K, von Neubeck C, Thames HD, Yaromina A, Dahm-Daphi J, et al. Residual gammaH2AX foci predict local tumour control after radiotherapy. Radiother Oncol 2013;108:434–9.

[44] Menegakis A, Eicheler W, Yaromina A, Thames HD, Krause M, Baumann M. Residual DNA double strand breaks in perfused but not in unperfused areas determine different radiosensitivity of tumours. Radiother Oncol 2011;100:137–44.
[45] Menegakis A, von Neubeck C, Yaromina A, Thames H, Hering S, Hennenlotter J. GammaH2AX assay in ex vivo irradiated tumour specimens: a novel method to determine tumour radiation sensitivity in patient-derived material. Radiother Oncol 2015.
[46] Bleeker FE, Molenaar RJ, Leenstra S. Recent advances in the molecular understanding of glioblastoma. J Neurooncol 2012;108:11–27.
[47] Holliday EB, Mitra HS, Somerson JS, Rhines LD, Mahajan A, Brown PD, et al. Postoperative proton therapy for chordomas and chondrosarcomas of the spine: adjuvant versus salvage radiation therapy. Spine 2015;40:544–9.
[48] Stupp R, Hegi ME, Mason WP, van den Bent MJ, Taphoorn MJ, Janzer RC, et al. Effects of radiotherapy with concomitant and adjuvant temozolomide versus radiotherapy alone on survival in glioblastoma in a randomised phase III study: 5-year analysis of the EORTC-NCIC trial. Lancet Oncol 2009;10:459–66.
[49] Zips D, Zophel K, Abolmaali N, Perrin R, Abramyuk A, Haase R, et al. Exploratory prospective trial of hypoxia-specific PET imaging during radiochemotherapy in patients with locally advanced head-and-neck cancer. Radiother Oncol 2012;105:21–8.
[50] Franzini A, Baty F, Macovei II, Durr O, Droege C, Betticher D. Gene expression signatures predictive of bevacizumab/erlotinib therapeutic benefit in advanced non-squamous non-small cell lung cancer patients (SAKK 19/05 trial). Clin Cancer Res 2015.
[51] Naipal KA, Verkaik NS, Ameziane N, van Deurzen CH, Ter Brugge P, Meijers M, et al. Functional ex vivo assay to select homologous recombination-deficient breast tumors for PARP inhibitor treatment. Clin Cancer Res 2014;20:4816–26.
[52] Shah MM, Dobbin ZC, Nowsheen S, Wielgos M, Katre AA, Alvarez RD, et al. An ex vivo assay of XRT-induced Rad51 foci formation predicts response to PARPinhibition in ovarian cancer. Gynecol Oncol 2014;134:331–7.
[53] West CM, Davidson SE, Burt PA, Hunter RD. The intrinsic radiosensitivity of cervical carcinoma: correlations with clinical data. Int J Radiat Oncol Biol Phys 1995;31:841–6.
[54] West CM, Davidson SE, Roberts SA, Hunter RD. The independence of intrinsic radiosensitivity as a prognostic factor for patient response to radiotherapy of carcinoma of the cervix. Br J Cancer 1997;76:1184–90.
[55] Rothkamm K, Barnard S, Ainsbury EA, Al-Hafidh J, Barquinero JF, Lindholm C, et al. Manual versus automated gamma-H2AX foci analysis across five European laboratories: can this assay be used for rapid biodosimetry in a large scale radiation accident? Mutat Res 2013;756:170–3.
[56] Runge R, Hiemann R, Wendisch M, Kasten-Pisula U, Storch K, Zophel K, et al. Fully automated interpretation of ionizing radiation-induced gammaH2AX foci by the novel pattern recognition system AKLIDES(R). Int J Radiat Biol 2012;88:439–47

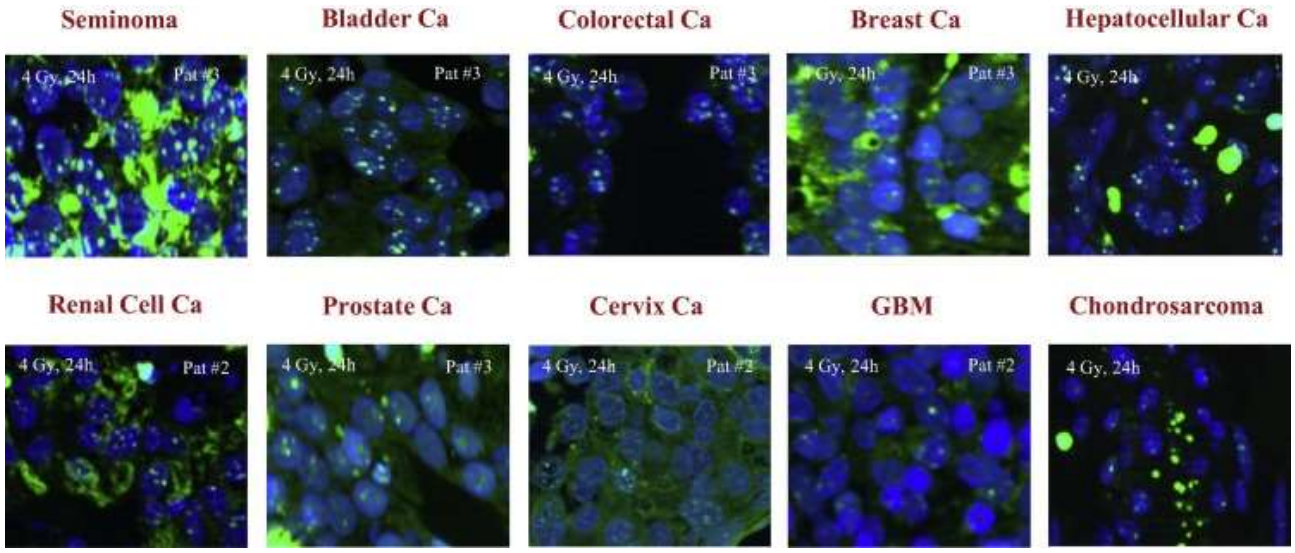

Fig. 1. Typical staining pattern of residual cH2AX foci: representative immunofluorescent images of residual cH2AX foci 24 h after 4 Gy ex vivo irradiation of patient-derived specimens are shown for each different tumour type included in the study. Original image magnification 400_. DNA DSB marker cH2AX foci in green (Alexa 488) and DNA counterstain in blue to visualize the cell nuclei (DAPI). Heterogeneity in the cell nuclear area can be observed (Table 1). The patient tumour sample used for the generation of the image, numbered according to Table 1 is also noted. The large cH2AX positive areas in some of the samples, e.g. seminoma, were not evaluated in the foci analysis and may represent either tumour cells in S phase, inflammatory cells or cells undergoing necrosis or apoptosis.

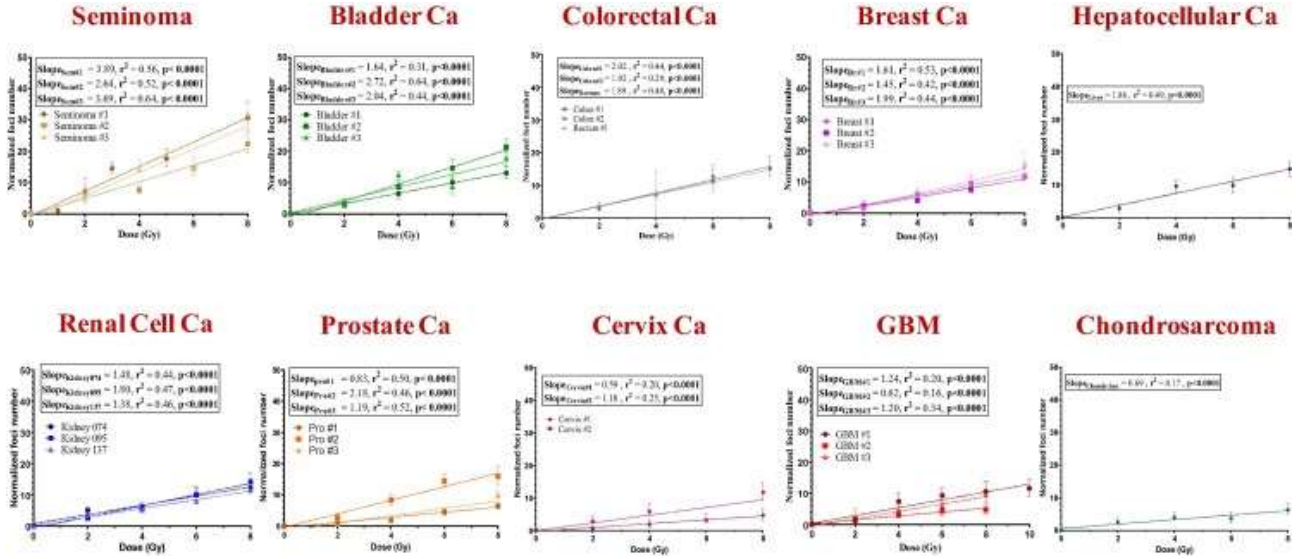

Fig. 2. Dose–response of residual cH2AX foci in ex vivo irradiated patient-derived tumour samples: linear regression analysis of residual cH2AX nfoci dose response across the different tumour types for each individual patient evaluated (Table 1). Patient-derived tumour specimen from different tumour types with known differences in clinical radiation sensitivity irradiated ex vivo with graded single doses after 24 h cultivation prior to irradiation. Symbols represent mean values of residual cH2AX nfoci quantified inat least 50 cells per dose level and error bars 95% confidence intervals. The parameters of the linear regression analysis (slope value, r-squared, p-value) for each patientderived specimen are noted. For cervix cancer #2 the sample irradiated with 6 Gy did not contain evaluable cells and was therefore omitted from the analysis.

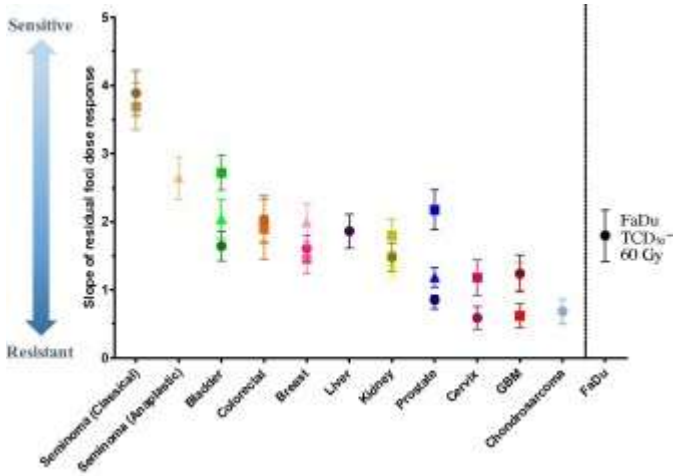

Fig. 3. The slope of the dose–response of the cH2AX nfoci in relation to the different tumour types with known differences in clinical radiation response. The slope value of each individual patient (Fig. 2) and 95% confidence intervals of the slope estimation are shown. The slope values, as marker of intrinsic radiation sensitivity of tumour cells, are well in line with the expected tumour-type specific differences of radio-responsiveness observed in the clinic after fractionatedradiation therapy.